Full-Wave Analysis of Dielectric-Loaded Cylindrical Waveguides and Cavities Using a New Four-Port Ring Network

Felipe L. Peñaranda-Foix, *Member, IEEE*, Michael D. Janezic, *Senior Member, IEEE*, Jose M. Catala-Civera, *Member, IEEE*, and Antoni J. Canos

***Abstract*—In this paper, a full-wave method for the electromagnetic analysis of dielectric-loaded cylindrical and coaxial waveguides and cavities is developed. For this purpose, a new four-port ring network is proposed, and the mode-matching method is applied to calculate the generalized admittance matrix of this new structure. A number of analyses on dielectric-loaded waveguide structures and cavities have been conducted in order to validate and to assess the accuracy of the new approach. The results have been compared with theoretical values, numerical modeling from the literature, and data from commercial electromagnetic simulators. The method has been also applied to the accurate determination of dielectric properties, and we provide an example of these measurements as another way to validate this new method.**

***Index Terms*—Circuit analysis, dielectric measurements, dielectric resonator, dielectric-loaded waveguides, electromagnetic modeling, microwave filter, mode matching (MM).**

I. Introduction

DIELECTRIC-LOADED waveguides and cavities are increasingly being employed in passive devices, such as microwave filters or dielectric resonators, that are integrated into satellite and mobile communications systems because of their small size, low loss, and temperature stability [1]. Dielectric materials also have many important functions in the microelectronics industry. For example, new packaging technologies require substrates with low permittivity. High-permittivity materials are used to reduce the dimensions of circuits at lower frequencies. Other important new areas of applications include microwave heating [2] and sensors [3]–[5].

This broad range of microwave applications demands a detailed knowledge of the dielectric properties of materials, including solids, liquids, emulsions, and powders [6]–[10]. As electrical components are miniaturized, the need for well-characterized dielectric measurements on materials increases [11], [12]. Dielectric properties measurement strategies include waveguide cells (in reflection or/and transmission), resonators, and free-space methods [13]–[16]. Dielectric-loaded cylindrical waveguides and cavities can provide new and accurate dielectric measurement procedures to be applied under these methodologies [17]–[20].

As a consequence, the study of dielectric inhomogeneities in waveguides and cavities has been a main task of microwave researchers over the last decades. The technical literature offers a large number of papers about the numerical solutions of the eigenmodes and eigenvectors of canonical metallic cavities loaded with dielectric resonators. The finite-element method (FEM) [21] and finite-difference time-domain (FDTD) [22] procedures have been primarily employed to solve this problem. The need to employ refined 3-D meshes and the frequency dependence of calculations make these methods very demanding in terms of computation time and memory resources.

To overcome these limitations, the mode-matching (MM) method [23]–[26] has emerged as an efficient and accurate technique to solve waveguide discontinuities and cavities. The boundary integral-resonant-mode expansion (BI-RME) technique [27], [28] has also been efficiently applied to the analysis of dielectric-loaded cavities of rectangular shape. For complex or large size waveguides or cavities, however, the MM method may suffer from convergence problems, and it has been combined with other analytical techniques [29]–[32]. Circuit analysis and segmentation have also proven to be powerful tools for analyzing complex dielectric-filled structures [33]–[35]. The generalized circuital analysis is a method for solving electromagnetic problems that consists of the segmentation of the whole geometry of the microwave structure into simpler elements, which then can be solved in an easier way [25], [36]–[41]. Once the simpler structures have been solved separately, they can be joined or combined through the use of the generalized admittance matrix (GAM) in order to give the complete solution of the complex structure.

In this paper, the calculation of the GAM matrix of a new four-port dielectric ring network is proposed. The term four-port does not refer to the terminals of the entire structure that is being analyzed. As shown in Fig. 2, this four-port ring network is only one of the elements, used in conjunction with other circuit elements, to model the larger structure. A four-port dielectric ring network is necessary because of the multiple dielectric layers that

Manuscript received February 27, 2012; revised June 14, 2012; accepted June 15, 2012. Date of publication July 12, 2012; date of current version August 28, 2012. This work was supported by the Ministry of Science and Innovation of Spain under Project MONIDIEL (TEC2008-04109). The work of F. L. Peñarada-Foix was supported by the Conselleria de Educación of the Generalitat Valenciana for economic support (BEST/2010/210).

F. L. Peñaranda-Foix, J. M. Catala-Civera, and A. J. Canos are with the Instituto de Aplicaciones de las Tecnologias de la Informacion y de las Comunicaciones Avanzadas (ITACA), Universidad Politécnica de Valencia, 46022 Valencia, Spain (e-mail: fpenaran@dcom.upv.es).

M. D. Janezic is with the National Institute of Standards and Technology (NIST), Boulder, CO 80305 USA.

Color versions of one or more of the figures in this paper are available online at http://ieeexplore.ieee.org.

Digital Object Identifier 10.1109/TMTT.2012.2206048

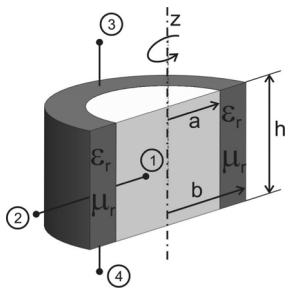

Fig. 1. Four-port ring network.

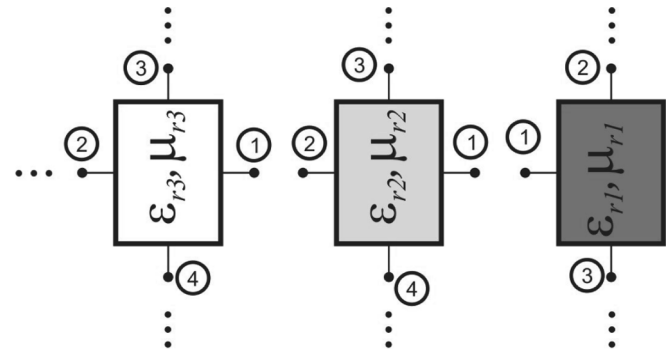

Fig. 2. Example of several four-port and three-port interconnection networks to model a multilayer structure.

can occur in both the radial (ports 1 and 2) and axial (ports 3 and 4) directions, as shown in Fig. 1. The GAM will be computed using the MM method, where the field in each port is approximated by a series expansion of basis functions. The set of basis functions has been chosen so that one can solve the resulting integrals analytically, without having to employ numerical methods. The combination of this new network with other circuit elements, such as cylindrical or coaxial waveguides, will allow an efficient and accurate tool to the full-wave solution of the scattering matrix or the resonant frequencies of dielectric-loaded cylindrical structures. Dielectric resonator filters and dielectric-filled re-entrant coaxial waveguides and cavities can be solved straightforwardly with the use of the developed full-wave analysis method. Moreover, the use of microwave cavities partially filled with two dielectrics shows a clear application of the method for measuring the dielectric properties of materials [42], [43].

The validity of the proposed four-port dielectric ring network is examined by modeling different well-known cylindrical transmission-line and cavity structures and then comparing the results with those included in the technical literature, as well as with those given by other numerical techniques. Measurements of some microwave devices are also included for validation purposes.

II. Theory

Fig. 1 shows the proposed four-port network to be analyzed. It consists of a toroid with inner radius a, outer radius b, and height h, with permittivity $\epsilon_r(\epsilon_r = \epsilon'\text{-}j\cdot\epsilon'')$ and permeability $\mu_r(\mu_r = \mu'\text{-}j\cdot\mu'')$. The four ports are defined as follows: port 1 at $r = a$, $0 \le z \le h$, port 2 at $r = b$, $0 \le z \le h$, port 3 at $a \le r \le b$, $z = h$ and port 4 at $a \le r \le b$, $z = 0$.

The four-port network can be combined with other networks by circuit analysis to model more complex structures. As an example, Fig. 2 shows how this four-port network can be interconnected to other three-port networks [44] to model a multilayer structure composed of several dielectric materials. The proposed circuit analysis enables the calculation of either the scattering parameters, in the case of a transmission-line structure, or the resonant frequencies for cavities or resonators.

The GAM of a four-port network is defined by the general expression (1)

$$\mathbf{Y} = \begin{pmatrix} \mathbf{Y}_{11} & \mathbf{Y}_{12} & \mathbf{Y}_{13} & \mathbf{Y}_{14} \\ \mathbf{Y}_{21} & \mathbf{Y}_{22} & \mathbf{Y}_{23} & \mathbf{Y}_{24} \\ \mathbf{Y}_{31} & \mathbf{Y}_{32} & \mathbf{Y}_{33} & \mathbf{Y}_{34} \\ \mathbf{Y}_{41} & \mathbf{Y}_{42} & \mathbf{Y}_{43} & \mathbf{Y}_{44} \end{pmatrix}. \tag{1}$$

It is important to note that each element in the GAM is a matrix that relates the modes in one port to the modes in remaining ports [26], [45], [46].

In general, the elements in (1) represent TEM, TM, or TE modes. However, the analysis described here is restricted to the TM modes with symmetry of revolution (TM_{0n}). Therefore, because of the particular geometry of the structures defined in Fig. 1, only TEM and TM modes are taken into account in the model. This restriction is strictly due to the type of the structures we are interested in, and it does not represent a loss of generality of the GAM technique. The procedure is, in fact, similar to the one followed in [47], where only TE_{0np} modes were employed to analyze the split post dielectric resonator.

With these assumptions, we define the components of the electromagnetic fields in the inner region $(a \le r \le b)$ as [48]

$$\begin{aligned} E_z &= \sum_{n=0}^{\infty} f_{0n}(r)\left(a_n e^{-\gamma_n z} + b_n e^{+\gamma_n z}\right) \\ E_r &= \sum_{n=0}^{\infty} \frac{-\gamma_n}{k_{c0n}} \cdot f'_{0n}(r)\left(a_n e^{-\gamma_n z} - b_n e^{+\gamma_n \cdot z}\right) \\ H_\varphi &= \sum_{n=0}^{\infty} \frac{-j\omega\varepsilon_0\varepsilon_r}{k_{c0n}} f'_{0n}(r)\left(a_n e^{-\gamma_{nz}} + b_n e^{+\gamma_{nz}}\right) \end{aligned} \tag{2}$$

where $f_{0n}(r)$ and $f'_{0n}(r)$ are

$$\begin{aligned} f_{0n}(r) &= \begin{cases} 0, & n = 0 \\ J_0(k_{c0n}r) + \Gamma_n Y_0(k_{c0n}r), & n > 0 \end{cases} \\ f'_{0n}(r) &= \begin{cases} \dfrac{-1}{(r\gamma_0)}, & n = 0 \\ -J_1(k_{c0n}r) - \Gamma_n Y_1(k_{c0n}r), & n > 0. \end{cases} \end{aligned} \tag{3}$$

In (3), the values of k_{c0n} (cutoff wavenumber) depend on the boundary conditions and the value of Γ_n. The mode $n = 0$ corresponds to the TEM mode, where $k_{c0n}|_{n=0} = 0$. However, in order to define (2) and (3) with more generality, and to include the TEM mode, the criteria of $k_{c00} = 1$ is adopted hereinafter.

The propagation constant γ_n and the cutoff wavenumber k_{c0n} are related as follows:

$$k_{c0n}^2 = k^2 + \gamma_n^2 \tag{4}$$

where k is the free-space wavenumber $k = \omega\sqrt{\varepsilon\mu}$.

The functions $J_n(\cdot)$ and $Y_n(\cdot)$ in (3) are, respectively, the Bessel functions of the first and second kind with order n (0

or 1), and Γ_n is a coefficient that depends on the boundary conditions.

Section II-A describes the calculation of the set of parameters $\mathbf{Y}_{i1}$, $(i = 1, 2, 3, 4)$ of (1).

A. Parameters $\mathbf{Y}_i 1$

To calculate the $\mathbf{Y}_{i1}$ parameters, electric wall conditions are imposed on ports 2–4, and therefore fields in (2) become

$$\left\{\begin{array}{l} E_r|_{z=0} = 0 \\ E_r|_{z=h} = 0 \\ E_z|_{r=b} = 0 \end{array}\right. \Rightarrow \left\{\begin{array}{c} a_n = b_n \\ \gamma_n = j\dfrac{n\pi}{h} \\ \Gamma_n = \dfrac{-J_0\left(k_{c0n}b\right)}{Y_0\left(k_{c0n}b\right)} \end{array}\right. . \tag{5}$$

By substituting the above relations in (2), the electromagnetic fields in the inner region are

$$\begin{aligned} E_z &= \sum_{n=0}^{\infty} 2a_n f_{0n}(r)\cosh(\gamma_n z) \\ E_r &= \sum_{n=0}^{\infty} 2a_n \frac{\gamma_n}{k_{c0n}} f'_{0n}(r)\sinh(\gamma_n z) \\ H_\varphi &= \sum_{n=0}^{\infty} 2a_n \frac{-j\omega\varepsilon_0\varepsilon_r}{k_{c0n}} f'_{0n}(r)\cosh(\gamma_n z). \end{aligned} \tag{6}$$

Given the propagation constant γ_n, the value of the cutoff wavenumbers can be calculated as

$$k_{c0n}^2 = k^2 + \gamma_n^2 = k^2 - \left(\frac{n\pi}{h}\right)^2. \tag{7}$$

In this case, the TEM mode does not exist because of the resulting geometry when short-circuiting ports 2–4. However, it must be noted that when computing the $\mathbf{Y}_{i3}$ and $\mathbf{Y}_{i4}$ parameters, the TEM mode does exist, and thus, it must be included.

The incident electric field at port 1 is

$$E_z = \sum_{m=0}^{\infty} \alpha_m \sin\left(2\pi m\frac{z}{h}\right) + \beta_m \cos\left(2\pi m\frac{z}{h}\right) \tag{8}$$

where we assume a Fourier series expansion, based on trigonometric basis functions, for this port.

Next, we equate (8) and the E_z field in (6) at $r = a$, and calculate the amplitudes a_n using the orthogonal properties of the trigonometric functions. We then obtain

$$a_n = \frac{\chi_n}{h f_{0n}(a)} \sum_{m=0}^{\infty} \alpha_m \cdot I_{mn}^{(s)} + \beta_m \cdot I_{mn}^{(c)} \tag{9}$$

where $I_{mn}^{(s)}, I_{mn}^{(c)}$, and χ_n are defined in the Appendix, Section A.

1) Parameter Y_{11}: In (10), the magnetic field at port 1 is written as a series expansion similar to the incident electric field defined in (8)

$$H_\varphi = \sum_{q=0}^{\infty} c_q \sin\left(2\pi q\frac{z}{h}\right) + d_q \cos\left(2\pi q\frac{z}{h}\right). \tag{10}$$

The magnetic field at port 1 and the inner magnetic field from (6) must be equal at $r = a$, which leads to the following expressions:

$$\begin{aligned} &\sum_{q=0}^{\infty} c_q \sin\left(2\pi q\frac{z}{h}\right) + d_q \cos\left(2\pi q\frac{z}{h}\right) \\ &\quad = \sum_{n=0}^{\infty} 2a_n \frac{-j\omega\varepsilon_0\varepsilon_r}{k_{c0n}} f'_{0n}(a)\cosh(\gamma_n z) \\ &\qquad\qquad \Downarrow \\ &c_q = \frac{2}{h}\sum_{n=0}^{\infty} 2a_n \frac{-j\omega\varepsilon_0\varepsilon_r}{k_{c0n}} f'_{0n}(a) I_{qn}^{(s)} \\ &d_q = \frac{2\chi_q}{h}\sum_{n=0}^{\infty} 2a_n \frac{-j\omega\varepsilon_0\varepsilon_r}{k_{c0n}} f'_{0n}(a) I_{qn}^{(c)}. \end{aligned} \tag{11}$$

Since parameter $\mathbf{Y}_{11}$ is defined as the relation between the electric and magnetic fields at port 1, we have

$$\mathbf{h}_1 = \begin{pmatrix} \mathbf{c} \\ \mathbf{d} \end{pmatrix} = \mathbf{Y}_{11} \cdot \mathbf{e}_1 = \begin{pmatrix} \mathbf{Y}_{11}^{(ss)} & \mathbf{Y}_{11}^{(sc)} \\ \mathbf{Y}_{11}^{(cs)} & \mathbf{Y}_{11}^{(cc)} \end{pmatrix} \cdot \begin{pmatrix} \boldsymbol{\alpha} \\ \boldsymbol{\beta} \end{pmatrix} \tag{12}$$

where each submatrix $\mathbf{Y}_{11}^{(xy)}$, being $(x, y) \in (s, c)$, is derived from (11) as follows:

$$Y_{11}^{(ss)}\big|_{qm} = \frac{2}{h}\sum_{n=0}^{\infty} \frac{-j\omega\varepsilon_0\varepsilon_r}{k_{c0n}} \frac{f'_{0n}(a)}{f_{0n}(a)} 2\chi_n \frac{I_{mn}^{(s)}}{h} I_{qn}^{(c)} \tag{13a}$$

$$Y_{11}^{(sc)}\big|_{qm} = 0 \tag{13b}$$

$$Y_{11}^{(cs)}\big|_{qm} = 0 \tag{13c}$$

$$Y_{11}^{(cc)}\big|_{qm} = \frac{2\chi_q}{h}\sum_{n=0}^{\infty} \frac{-j\omega\varepsilon_0\varepsilon_r}{k_{c0n}} \frac{f'_{0n}(a)}{f_{0n}(a)} 2\chi_n \frac{I_{mn}^{(c)}}{h} I_{qn}^{(c)}. \tag{13d}$$

2) Parameter $\mathbf{Y}_{21}$: The calculation of parameter $\mathbf{Y}_{21}$ is obtained in a similar way to the $\mathbf{Y}_{11}$ parameter, noting that port 2 is now placed at $r = b$.

3) Parameter $\mathbf{Y}_{31}$: The magnetic field at port 3 is written as a series expansion of the basis functions $h_q^{(3)}(r)$

$$H_\varphi = \sum_{q=0}^{\infty} c_q h_q^{(3)}(r) = \sum_{q=0}^{\infty} c_q \omega_{1q}^{(3)}(r) N_q^{(e3)}, \qquad a \le r \le b \tag{14}$$

where the basis functions $h_q^{(3)}(r)$ used at port 3 and at port 4 are orthogonal in the range $a \le r \le b$. They are a complete set of Bessel functions, which makes them suitable for structures that can be described in circular-cylindrical coordinates. The series expansion used is a generalization of the Dini series expansions [49] as they were developed in [50]. This series expansion is included in Appendix, Section B (superindex$^{(3)}$ in function $\omega_{1q}^{(3)}(r)$ refers to port 3). The term $N_q^{(e3)}$ is a normalization term for the electric field [51], [52]. This term is also calculated in the Appendix, Section C.

By equating the magnetic field at port 3 with the inner magnetic field, defined in (6), over the region $z = h$, we get

$$\sum_{q=0}^{\infty} c_q \omega_{1q}^{(3)}(r) N_q^{(e3)} = \sum_{n=0}^{\infty} 2a_n \frac{-j\omega\varepsilon_0\varepsilon_r}{k_{c0n}} f'_{0n}(r)\cosh(\gamma_n h)$$
$$\Downarrow$$
$$c_q = \frac{1}{B_q^{(3)} N_q^{(e3)}} \sum_{n=0}^{\infty} 2a_n \frac{-j\omega\varepsilon_0\varepsilon_r}{k_{c0n}} \cos(n\cdot\pi) I_{qn}^{(\omega)} \quad (15)$$

where $N_q^{(e3)}$ has been defined in (37), $B_q^{(3)}$ has been defined in (34), and $I_{qn}^{(\omega)}$ is defined in the Appendix, Section D.

Defining the parameter $\mathbf{Y}_{31}$ as the relation between the magnetic field at port 3 and electric field at port 1, we have

$$\mathbf{h}_3 = \mathbf{c} = \mathbf{Y}_{31}\cdot\mathbf{e}_1 = \left(\mathbf{Y}_{31}^{(s)} \quad \mathbf{Y}_{31}^{(c)}\right)\cdot\begin{pmatrix}\boldsymbol{\alpha}\\ \boldsymbol{\beta}\end{pmatrix} \quad (16)$$

where each submatrix $\mathbf{Y}_{31}^{(x)}$, being $(x) \in (s, c)$ is from (15)

$$Y_{31}^{(s)}\big|_{qm} = \frac{1}{B_q^{(3)} N_q^{(e3)}} \cdot \sum_{n=0}^{\infty} \frac{-j\omega\varepsilon_0\varepsilon_r}{k_{c0n}} 2\chi_n \frac{\cos(n\pi)}{f_{0n}(a)} \frac{I_{mn}^{(s)}}{h} I_{qn}^{(\omega)} \quad (17a)$$

$$Y_{31}^{(c)}\big|_{qm} = \frac{1}{B_q^{(3)} N_q^{(e3)}} \cdot \sum_{n=0}^{\infty} \frac{-j\omega\varepsilon_0\varepsilon_r}{k_{c0n}} 2\chi_n \frac{\cos(n\pi)}{f_{0n}(a)} \frac{I_{mn}^{(c)}}{h} I_{qn}^{(\omega)}. \quad (17b)$$

4) Parameter $\mathbf{Y}_{41}$*:* The calculation of parameter $\mathbf{Y}_{41}$ is obtained in a similar manner to the $\mathbf{Y}_{31}$ parameter, but in the region $z = 0$.

B. Parameters $\mathbf{Y}_{i2}$*,* $\mathbf{Y}_{i3}$*, and* $\mathbf{Y}_{i4}$

Since the remaining parameters of columns 2–4 of the Y-matrix are calculated in a similar way to the parameters in the first column, Y_{i1}, we do not include here (for the sake of space) how their expressions are determined.

C. Losses in the Electric Walls

Dielectric or magnetic losses of the material in the ring circuit of Fig. 1 are included in the imaginary parts of the complex permittivity and complex permeability, respectively, as defined previously, but the conductive losses associated with the electric walls requires an additional explanation. The impedance associated with a finite conductivity electric wall can be calculated with the well-known expression [53]–[55]

$$Z_{short} \approx R_s(1+j), R_s = \frac{1}{\sigma\delta} = \sqrt{\frac{\pi f\mu}{\sigma}}. \quad (18)$$

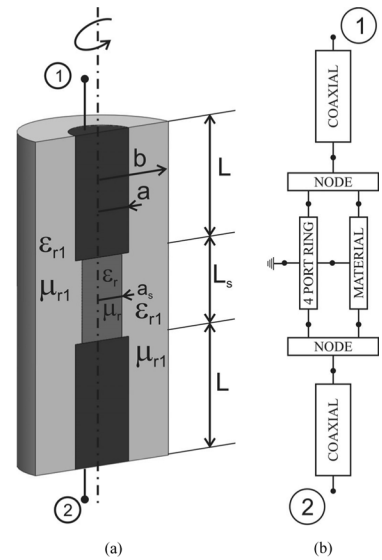

Fig. 3. Re-entrant coaxial waveguide and its circuit segmentation.

The same expression can be retrieved from the computed GAM matrix. Assuming $b \to \infty$, we obtain a one-port element where the unique GAM parameter is Y_{11}. From the second Maxwell equation, a good dielectric satisfies $\sigma/(\omega\varepsilon) << 1$ and a good conductor satisfies $\sigma/(\omega\varepsilon) >> 1$ (see [48] and [56]). Thus, for a good conductor, we can assume that the following permittivity relationship applies:

$$\varepsilon = \frac{-j\sigma}{\omega}. \quad (19)$$

The open-space wavenumber k associated with this permittivity is

$$k^2 = \omega^2\mu\varepsilon = -j\omega\mu\sigma \Rightarrow k = \frac{1-j}{\delta} \quad (20)$$

where δ is the penetration depth used in (18). Using (20) in parameter $\mathbf{Y}_{11}$, we obtain the following expression:

$$\frac{f'_{0n}(a)}{f_{0n}(a)} = \left.\frac{-J_1(k_{c0n}a) + \dfrac{J_0(k_{c0n}b)}{Y_0(k_{c0n}b)} Y_1(k_{c0n}a)}{J_0(k_{c0n}a) - \dfrac{J_0(k_{c0n}b)}{Y_0(k_{c0n}b)} Y_0(k_{c0n}a)}\right|_{b\to\infty} \approx -\frac{H_1^{(2)}(k_{c0n}a)}{H_0^{(2)}(k_{c0n}a)} \quad (21)$$

where the cutoff wavenumber k_{c0n} is (7)

$$k_{c0n}^2 = k^2 + \gamma_n^2 = \omega^2\mu\varepsilon - \left(\frac{n\pi}{h}\right)^2 = -j\omega\mu\sigma - \left(\frac{n\pi}{h}\right)^2. \quad (22)$$

For most metals, the value of the conductivity σ is relatively high so the expression for the wavenumber can be approximated by

$$k_{c0n}^2 \approx -j\omega\mu\sigma. \quad (23)$$

With respect to $\mathbf{Y}_{11}$, we then have

$$Y_{11}^{(ss)}\big|_{qm} \approx \frac{-1}{1+j}\frac{1}{R_s}\delta(m-q) \quad (24a)$$

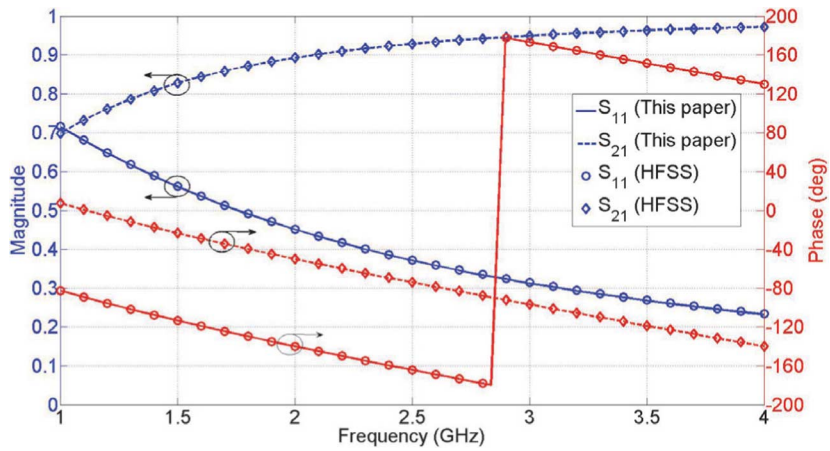

Fig. 4. Magnitude and phase of the S-parameters with air gap when $a = 7.25$ mm, $b = 24.9$ mm, $a_s = 10$ mm, $L_s = 2$ mm, $L = 15$ mm, and $\epsilon_r = 1$.

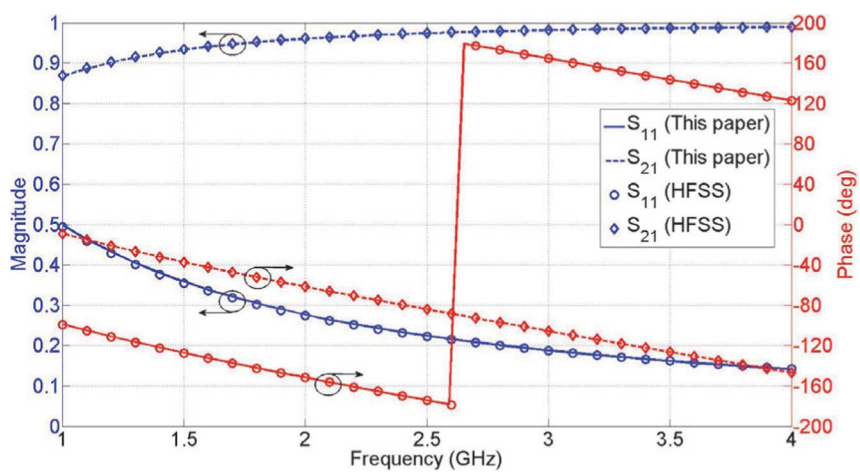

Fig. 5. Magnitude and phase of the S-parameters with air gap when $a = 7.25$ mm, $b = 24.9$ mm, $a_s = 10$ mm, $L_s = 2$ mm, $L = 15$ mm, and $\epsilon_r = 2\text{-}j\cdot 0.002$.

$$Y_{11}^{(sc)}\big|_{qm} = 0 \tag{24b}$$

$$Y_{11}^{(cs)}\big|_{qm} = 0 \tag{24c}$$

$$Y_{11}^{(cc)}\big|_{qm} \approx \frac{-1}{1+j}\frac{1}{R_s}\delta\left(m-q\right) \tag{24d}$$

where $\delta(\cdot)$ is the Dirac delta function. As expected, the one-port network GAM for the finite conductive electric wall results in a diagonal matrix with the impedance value of (18). The sign discrepancy comes from the Poynting vector flux that in this paper is outgoing from the network and not ingoing as usual. Applying this standard criterion, the sign of the magnetic field changes, which also changes the sign of the GAM, leading to the same value for (18).

III. Numerical Results and Discussion

In order to validate the accuracy of the numerical model described in Section II, and demonstrate the usefulness of the combination of this new four-port network with cylindrical or coaxial waveguides, modeling results of typical dielectric-loaded microwave structures are compared with analytical expressions, general-purpose FEM simulators, and with results previously published in the literature. This is shown in Sections III-A–III-D. Section III-E includes an example of permittivity measurements as illustrative of another application of the proposed network.

A. Coaxial Waveguide Loaded With a Dielectric Disk

Fig. 3(a) shows a coaxial waveguide with a cylindrical dielectric sample positioned between the two inner conductors. Fig. 3(b) shows how this structure is broken down into different networks, where the proposed four-port ring network is combined with one-port (short-circuit), two-port (coaxial line), and three-port (node) networks (see [33] and [44] for details of this networks).

Figs. 4 and 5 show the magnitude and phase of the S-parameters of the two-port structure calculated by joining the nodes and networks described in Fig. 3(b) for a dielectric disc of permittivity of air and permittivity of $\epsilon_r = 2\text{-}j\cdot 0.002$, respectively. Dimensions of the geometry are given in the figure caption. Only 15 modes over 50 frequency points were required to solve the dielectric-loaded coaxial in less than 6 s with a PC (Intel Core i5-2320 and 6-GB RAM). The computed results (labeled MODAL) are in very good agreement with those provided by the commercial code Ansoft HFSS (labeled HFSS) also included in the figures for comparison. Of course,

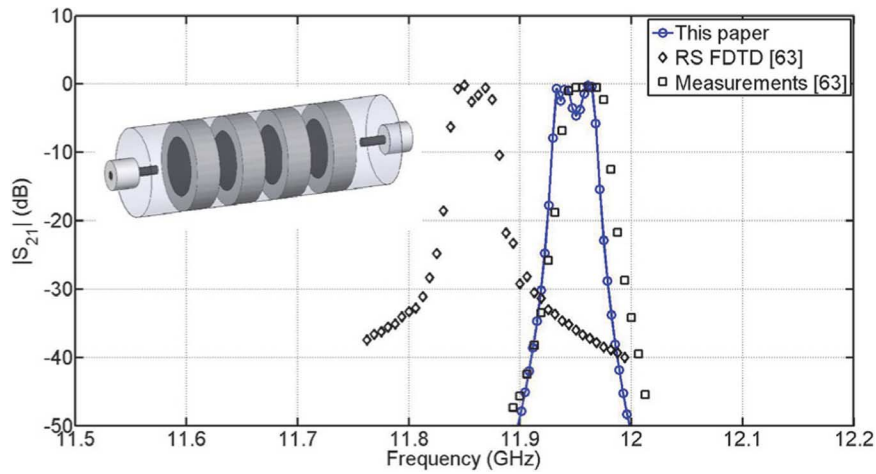

Fig. 6. Four-pole TM_{01} DR filter (see dimensions in [63]).

the accuracy of the modeling depends on the number of modes selected to perform the calculations. The number of modes has a direct impact on the required processing time. In this, and in the rest of the simulated cases, good accuracy has been reached, when compared with references in the literature, by selecting only a few modes (i.e., 15 modes in this first example), which allows one to analyze the structures in a reasonable amount of time.

By short circuiting (perfect electric walls are assumed in the simulation) both ends (ports 1 and 2), and imposing resonant condition [57], this structure becomes a re-entrant cavity, which is a common device for measuring the complex permittivity of dielectric materials, as described in [29] and [58]–[62].

B. Cylindrical Dielectric Resonant (DR) Filters

The second structure considered is a four-pole TM_{01} DR filter shown in Fig. 6 [63]. It consists of a set of spaced dielectric-loaded cylindrical waveguides coupled by coaxial lines. The dielectric support of the dielectric resonator has a relative permittivity of 1.031, and the rest of parameters are given in the figure caption. To solve for the S-parameters of this structure, the schematic of Fig. 6 is segmented by connecting the nodes of the four-port network to cylindrical waveguides in a similar manner to the coaxial of Fig. 3.

The computed S-parameters for the four-pole filter are shown in Fig. 6. To obtain an accurate S-parameters over 150 frequency points, we included 30 modes, which resulted in a total computation time of 60 s using a laptop (Intel Core i5 and 6-GB RAM). The computed performance of the four-pole filter is compared in Fig. 6 with simulations and measurements of the same structure carried out in [63]. Very good agreement with measurements is observed from the figure.

C. Cylindrical Cavity Coaxially Loaded With Two Dielectric Materials

The third structure to be studied with the proposed method is a cylindrical cavity coaxially loaded with two dielectric materials that extends along the cavity height, as shown in Fig. 7. This inhomogeneous cavity can be solved analytically, giving us the opportunity to compare the accuracy of the

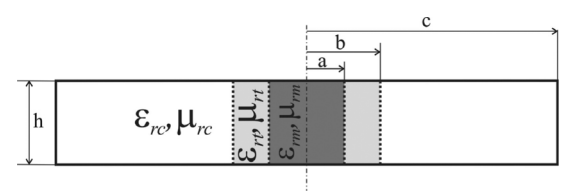

Fig. 7. Coaxially loaded cavity with container.

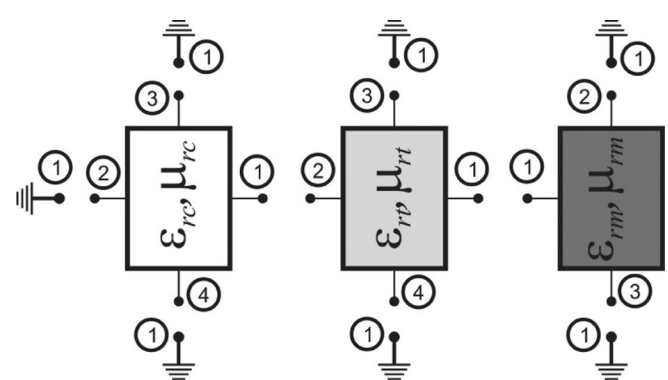

Fig. 8. Circuit segmentation of a coaxially loaded cavity.

proposed model with previously published analytical results. For this configuration, ports 1 and 2 of the four-port network are joined with the materials in contact, whereas ports 3 and 4 are short circuited (see Fig. 8). The three-port network of Fig. 8 is described in [44]. Short circuits can be modeled either as perfect electric conductors (PECs) or conductors with a finite conductivity, as described previously in Section II. Resonant frequencies and quality factors have been calculated using the resonant condition [57] and the complex resonant frequency concept [56].

Table I shows the first two resonant frequencies and Q factors corresponding to the TM_{0np} (TM_{010} and TM_{020}) modes of a cylindrical cavity coaxially loaded with dielectric materials of different permittivity, and first resonant mode TM_{010} when the dielectric is inside a dielectric tube. In both cases (with and without a tube), the calculated values are identical to those provided by an analytical solution of this structure [48] so that we

TABLE I
RESONANT FREQUENCY COMPARISONS $a = 15$ mm, $b = 20$ mm, $c = 50$ m, $h = 20$ mm

		f (GHz)	Q
MODE 1 ε_{rm}=2·(1-j·10^{-2}) ε_{rtf}=2·(1-j·10^{-2})	Analytic	1.8736	144.536
	This paper	1.8736	144.536
	HFSS	1.8988	144.466
MODE 2 ε_{rm}=2·(1-j·10^{-2}) ε_{rtf}=2·(1-j·10^{-2})	Analytic	4.5788	265.069
	This paper	4.5788	265.069
	HFSS	4.6409	264.948
MODE 1 ε_{rm}=5·(1-j·10^{-4}) ε_{rtf}=5·(1-j·10^{-4})	Analytic	1.3020	11444.3
	This paper	1.3020	11444.3
	HFSS	1.3192	11442.2
MODE 2 ε_{rm}=5·(1-j·10^{-4}) ε_{rtf}=5·(1-j·10^{-4})	Analytic	3.7356	16965.3
	This paper	3.7356	16965.3
	HFSS	3.7857	19938.0
MODE 1 ε_{rm}=5·(1-j·10^{-4}) ε_{rtf}=2·(1-j·10^{-2})	Analytic	1.4322	698.79
	This paper	1.4322	698.79
	HFSS	1.4515	698.88

can assess the accuracy and performance of this technique. In order to compare with the analytic solutions, the conductivity of the walls is assumed infinite ($\sigma = \infty$). In all the cases, the resonant frequencies provided by the Ansoft HFSS simulations are included, and the relative errors are about 1.3% in the resonant frequencies and 0.05% in the quality factors.

D. Cylindrical Cavity Partially Loaded With a Dielectric Disk

The next structure analyzed is a cylindrical cavity partially filled with a dielectric disc that can be located at different height [see Fig. 9(a)]. This cavity can be split into simple circuit elements, as shown in Fig. 9(b), where the four-port ring network is connected to the other four-port ring networks (up and down) and terminated with short circuits [44].

Fig. 10 shows the calculated resonant frequencies of the first two modes (TM_{01} and TM_{02}) as a function of the rate between the cavity height and the dielectric disk diameter when the material is placed at the bottom ($h_d = 0$) and for a given value of permittivity (comb-line resonator). For comparison, the figure also reproduces the results given by [64] of the same structure, showing again very good agreement between both approaches.

The cavity loaded with the dielectric disk at the center ($h_d = h_u$), as represented in Fig. 9(a), has been extensively used in the

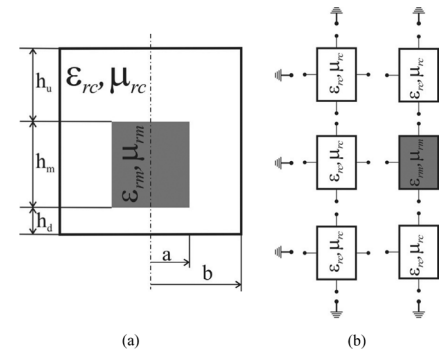

Fig. 9. Cylindrical cavity partially loaded with: (a) a dielectric disk and (b) circuit segmentation.

TABLE II
SIMULATIONS OF RESONANT FREQUENCIES (IN GIGAHERTZ) $\epsilon_r = 35.74$, $a = 0.8636$ cm, $b = 1.295$ cm, $h_m = 0.762$ cm, $h_u = h_d = 0.381$ cm

Mode	[1]	[65]	This paper	Relative error (%) with [1] and [65] respectively
TM_{01}	4.568	4.5442	4.5410	0.60 0.07
TM_{02}	6.384	6.361	6.3732	0.17 -0.19
TM_{03}	7.323	7.254	7.2622	0.84 -0.11
TM_{04}	7.685	7.641	7.6614	0.31 -0.27
TM_{05}	9.169	9.093	9.1078	0.67 -0.16
TM_{06}	10.031	9.942	9.9827	0.48 -0.41

literature to compare different methods of analysis. Therefore, we compare our results with those obtained by the orthonormal basis method [1] and with the MM method of [65]. Table II presents a list with some of these results corresponding to the TM_{0n} modes. Again, we find excellent agreement between our results and those using other approaches, which confirm the validity of the developed method (the conductivity is assumed to be infinite because no information about it is provided in the references).

In order to compute each resonant frequency, the Nelder–Mead minimization method was used [66], with an average of 180 evaluations when we included 30 modes, resulting in a computation time of 180 s per frequency point.

E. Dielectric Measurements With Cylindrical Cavity Partially Loaded With a Dielectric Disk

Finally, we included an example of permittivity measurements of a dielectric disk in the cylindrical cavity depicted in Fig. 9(a) with $h_d = 0$. Table III shows the measurements of the resonant frequency and Q factor of the cylindrical cavity containing samples of ceramic materials (with high- and low-permittivity values) and the calculated permittivity of the samples using the circuital representation of Fig. 9(b). Resonance measurements have been carried out following the procedures described in [67]. Dimensions of cavity and

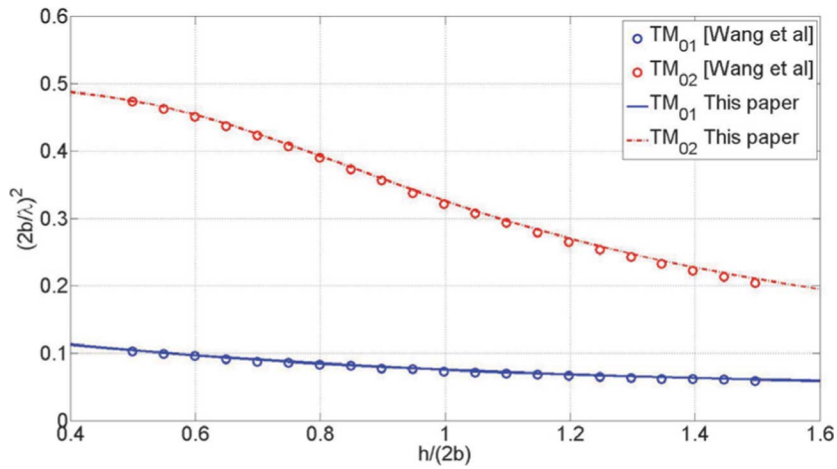

Fig. 10. Resonant frequency of the first two TM modes with $a/b = 0.3$, $a = 20$ mm, $h_m/h = 0.9$, and $\epsilon_r = 36$.

TABLE III
PERMITTIVITY MEASUREMENTS OF TRANS-TECH MATERIALS $b = 49.07$ mm, $h_{\text{Total}} = 20$ mm, $h_d = 0$ mm, $\sigma = 0.955 \cdot 10^7$ S/m

Material dimensions	Meas. f_r [GHz]	Meas. Q	ε_r		
			Data sheet	This paper	NIST
D8623 a=29.83 mm h_m=3.36 mm	2.09567	2819	75	75.09-j·0.0020	79.6
D6 a=29.83 mm h_m=5.98 mm	2.03163	3510	6.3	6.54-j·0.0026	6.59

samples are also given in the table, as well as the measured conductivity, which is determined through a measurement of the empty cavity.

The calculated results show very good agreement with the values provided by the material manufacturer's data sheet and with other measurements performed in a split-cylinder resonator at the National Institute of Standards and Technology (NIST), Boulder, CO, thereby confirming the validity of the developed approach to accurately measure the dielectric properties of materials.

IV. CONCLUSION

In this paper, the GAM of a novel four-port cylindrical ring network has been successfully solved. The combination of the proposed ring circuit network with coaxial and cylindrical waveguides can be used to model a variety of complex structures. For instance, they have been used for solving dielectric-loaded structures widely employed as microwave devices and resonators, including those with finite conductivity walls.

This new element has been used to calculate the S-parameters, resonant frequencies, and quality factor of some dielectric loaded structures with dielectric disks.

The results provided by this new element have been compared with theoretical results, as well as with data included in the technical literature, with commercial FEM software values, and with measurements, showing very good agreement in all cases.

APPENDIX

Values of $I_{mn}^{(s)}$ and $I_{mn}^{(c)}$ in (9): Integrals $I_{mn}^{(s)}$ and $I_{mn}^{(c)}$ are

$$\begin{aligned} I_{mn}^{(s)} &= \int_{z=0}^{h} \cosh(\gamma_n z) \sin\left(2\pi m \frac{z}{h}\right) dz \\ &= -\pi m h \operatorname{sinc}\left(\frac{n}{2}+m\right) \operatorname{sinc}\left(\frac{n}{2}-m\right) \end{aligned} \tag{25a}$$

$$\begin{aligned} I_{mn}^{(c)} &= \int_{z=0}^{h} \cosh(\gamma_n z) \cos\left(2\pi m \frac{z}{h}\right) dz \\ &= \frac{h}{2\chi_m} \delta(n-2m) \end{aligned} \tag{25b}$$

and χ_n is defined as

$$\chi_n = \begin{cases} \frac{1}{2}, & m = 0 \\ 1, & m \neq 0. \end{cases} \tag{26}$$

Basis Functions Used in Port 3: The basis functions used for the series expansion at port 3 [see magnetic field in port 3 in (14)] and port 4 are based on a generalization of the Dini series expansion [49] as reported in [50].

The general expression for the series expansion of a function $f(r)$ is

$$f(r) = \sum_{m=0}^{\infty} \frac{c_m}{B(\mu_m)} \Phi_\nu(\mu_m r, \mu_m a), \qquad a \leq r \leq b \tag{27}$$

where order ν is an arbitrary value and where the weights of the series expansion are

$$\begin{aligned} c_m &= \int_{r=a}^{b} r f(r) \Phi_\nu(\mu_m r, \mu_m a) dr \\ B(\mu_m) &= \int_{r=a}^{b} r \Phi_\nu^2(\mu_m r, \mu_m a) dr. \end{aligned} \tag{28}$$

The basis function $\Phi_\nu(\mu_m r, \mu_m a)$ is

$$\Phi_\nu(\mu_m r, \mu_m a) = \mu_m h_1 f_{1\nu}(\mu_m r, \mu_m a) - f_{2\nu}(\mu_m r, \mu_m a) \tag{29a}$$

$$\begin{aligned} f_{1\nu}(\mu_m r, \mu_m a) = \frac{\pi \mu_m a}{2} \big[& Y_\nu'(\mu_m a) J_\nu(\mu_m r) \\ & - J_{-\nu}'(\mu_m a) \cdot Y_\nu(\mu_m r) \big] \end{aligned} \tag{29b}$$

$$f_{2\nu}\left(\mu_m r, \mu_m a\right) = \frac{-\pi\mu_m a}{2}\left[Y_\nu\left(\mu_m a\right) J_\nu\left(\mu_m r\right) - J'_\nu\left(\mu_m a\right) Y_\nu\left(\mu_m r\right)\right]. \quad (29c)$$

Following these definitions, the series expansion in (27) is then true if

$$\Phi_\nu\left(\mu_m r, \mu_m a\right) + h_1 \frac{\partial \Phi_\nu\left(\mu_m r, \mu_m a\right)}{\partial r}\bigg|_{r=a} = 0$$
$$\Phi_\nu\left(\mu_m r, \mu_m a\right) + h_2 \frac{\partial \Phi_\nu\left(\mu_m r, \mu_m a\right)}{\partial r}\bigg|_{r=b} = 0. \quad (30)$$

The first equation is always true (and can be easily proven) and the second one implies that, for a given h_1 and h_2,

$$\mu_m h_2 \left[\begin{array}{c}\mu_m h_1 f'_{1\nu}\left(\mu_m b, \mu_m a\right) - \\ f'_{2\nu}\left(\mu_m b, \mu_m a\right)\end{array}\right] + \left[\mu_m h_1 f_{1\nu}\left(\mu_m b, \mu_m a\right) - f_{2\nu}\left(\mu_m b, \mu_m a\right)\right] = 0. \quad (31)$$

The zeros of this equation are the parameters μ_m used in the series expansion. In our case, we are using $\nu = 1$ and $h_1 = a$ and $h_2 = b$, and then the basis function is

$$\begin{aligned}\Phi_1\left(\mu_m r, \mu_m a\right) &= \omega_{1m}\left(r\right) \\ &= \frac{\pi\mu_m^2 a^2}{2} \\ &\quad \cdot \left[J_1\left(\mu_m r\right) Y_0\left(\mu_m a\right) - J_0\left(\mu_m a\right) Y_1\left(\mu_m \cdot r\right)\right] \end{aligned} \quad (32)$$

where the function $\omega_{1m}(r)$ has been defined, and used in (14), and where μ_m are the zeros of

$$\begin{aligned}\omega_{0m}\left(b\right) &= \frac{\pi\mu_m^2 a^2}{2} \\ &\quad \cdot \left[J_0\left(\mu_m b\right) Y_0\left(\mu_m a\right) - J_0\left(\mu_m a\right) Y_0\left(\mu_m b\right)\right] \\ &= 0. \end{aligned} \quad (33)$$

It is important to remark that, apart from the trivial zero $\mu_0 = 0$, the rest of the zeros are the cutoff wavenumbers of TM_{0m} modes in the coaxial waveguide.

Finally, term $B(\mu_m)$, the normalization term in (28), is

$$B\left(\mu_m\right) = \begin{cases} \dfrac{a^4\mu_m^2}{2}\ln\left(\dfrac{b}{a}\right), & m = 0 \\ \dfrac{a^4\mu_m^2}{2}\left[-1 + \left(\dfrac{J_0\left(\mu_m a\right)}{J_0\left(\mu_m b\right)}\right)^2\right], & m > 0 \end{cases} \quad (34)$$

and it is important to note the 0 in the origin ($\mu_m = 0, m = 0$), where function $\omega_{1m}(r)$ is

$$\omega_{1m}\left(r\right)\big|_{m=0} = \frac{a^2\mu_m}{r} \quad (35)$$

where the coefficient c_m, $m = 0$, in the series expansion is

$$c_0 = a^2\mu_m \int_{r=a}^{b} f\left(r\right) dr. \quad (36)$$

Note that this case is the TEM mode.

Normalization Term $N_q^{(e3)}$: $N_q^{(e3)}$ is a normalization term for the electric field [51], [52] and is calculated as

$$\begin{aligned}&\int_{r=a}^{b} h_q^{(3)}\left(r\right) h_m^{(3)}\left(r\right) r dr \\ &\quad = \int_{r=a}^{b} \omega_{1q}^{(3)}\left(r\right) N_q^{(e3)} \omega_{1m}^{(3)}\left(r\right) N_m^{(e3)} r dr \\ &\quad = \delta_{mq} \\ &\qquad \Downarrow \\ &N_q^{(e3)} = \begin{cases} \dfrac{1}{a^2\mu_0\sqrt{\ln\left(\dfrac{b}{a}\right)}}, & q = 0 \\ \dfrac{\sqrt{2}}{a^2\mu_q\sqrt{-1 + \left(\dfrac{J_0\left(\mu_m a\right)}{J_0\left(\mu_m b\right)}\right)^2}}, & q \neq 0. \end{cases} \end{aligned} \quad (37)$$

Value of Integral $I_{qn}{}^{(\omega)}$ in (15): Integral $I_{qn}^{(\omega)}$ is

$$\begin{aligned} I_{qn}^{(\omega)} &= \int_{r=a}^{b} f'_{0n}\left(r\right) \cdot \omega_{1q}^{(3)}\left(r\right) \cdot r \cdot dr \\ &= \begin{cases} \dfrac{-a \cdot k_{c0n}}{k_{c0n}^2 - k_{c0q}^2} \cdot f_{0n}\left(a\right) \cdot \omega_{1q}^{(3)}\left(a\right), & q > 0 \\ \dfrac{-a^2 \cdot f_{0n}\left(a\right)}{k_{c0n}}, & q = 0. \end{cases} \end{aligned} \quad (38)$$

REFERENCES

[1] J. A. Monsoriu, M. V. Andrés, A. Silvestre, A. Ferrando, and B. Gimeno, "Analysis of dielectric-loaded cavities using an orthonormal-basis method," *IEEE Trans. Microw. Theory Tech.*, vol. 50, no. 11, pp. 2545–2552, Nov. 2002.

[2] S. Charmond, C. P. Carry, and D. Bouvard, "Densification and microstructure evolution of Y-tetragonal zirconia polycrystal powder during direct and hybrid microwave sintering in a single-mode cavity," *J. Eur. Ceram. Soc.*, vol. 30, no. 6, pp. 1211–1221, 2010.

[3] T. Baum, L. Thompson, and K. Ghorbani, "Complex dielectric measurements of forest fire ash at X-band frequencies," *IEEE Geosci. Remote Sens. Lett.*, vol. 8, no. 5, pp. 859–863, Sep. 2011.

[4] S. Hausman, L. Januszkiewicz, M. Michalak, T. Kacprzak, and I. Krucinska, "High frequency dielectric permittivity of nonwoven," *Fibres & Textiles Eastern Eur.*, vol. 14, no. 5, pp. 60–63, Jan./Dec. 2006.

[5] T. Oguchi, M. Udagawa, N. Nanba, M. Maki, and Y. Ishimine, "Measurements of dielectric constant of volcanic ash erupted from five volcanoes in japan," *IEEE Trans. Geosci. Remote Sens.*, vol. 47, no. 4, pp. 1089–1096, Apr. 2009.

[6] R. Renoud, C. Borderon, and H. W. Gundel, "Measurement and modeling of dielectric properties of Pb(Zr,Ti)O3 ferroelectric thin films," *IEEE Trans. Ultrason., Ferroelectr., Freq. Control*, vol. 58, no. 9, pp. 1975–1980, Sep. 2011.

[7] M. Zhang, J. Zhai, and X. Yao, "Microwave dielectric properties of high dielectric tunable—Low Permittivity Ba0.5Sr0.5TiO3–Mg2(Ti0.95Sn0.05)O4 composite ceramics," *Ceramics Int.*, vol. 38, pp. S173–S176, Jan. 2012, Suppl. 1.

[8] C. C. Khaw, K. B. Tan, and C. K. Lee, "High temperature dielectric properties of cubic bismuth zinc tantalate," *Ceramics Int.*, vol. 35, no. 4, pp. 1473–1480, May 2009.

[9] A. Chaouchi, S. d'Astorg, and S. Marinel, "Low sintering temperature of (Zn0.65Mg0.35)TiO3-xCaTiO3-based dielectric with controlled temperature coefficient," *Ceramics Int.*, vol. 35, no. 5, pp. 1985–1989, Jul. 2009.

[10] D. L. Guerra, S. P. Oliveira, R. A. S. Silva, E. M. Silva, and A. C. Batista, "Dielectric properties of organofunctionalized kaolinite clay and application in adsorption mercury cation," *Ceramics Int.*, vol. 38, no. 2, pp. 1687–1696, Mar. 2012.

[11] J. Krupka and W. Gwarek, "Measurements and modeling of planar metal film patterns deposited on dielectric substrates," *IEEE Microw. Wireless Compon. Lett.*, vol. 19, no. 3, pp. 134–136, Mar. 2009.

[12] J. Krupka, W. Gwarek, N. Kwietniewski, and J. G. Hartnett, "Measurements of planar metal-dielectric structures using split-post dielectric resonators," *IEEE Trans. Microw. Theory Tech.*, vol. 58, no. 12, pp. 3511–3518, Dec. 2010.

[13] J. Baker-Jarvis, M. Janezic, and D. Degroot, "High-frequency dielectric measurements," *IEEE Instrum. Meas. Mag.*, vol. 13, no. 2, pp. 24–31, Apr. 2010.

[14] U. Kaatze and C. Hübner, "Electromagnetic techniques for moisture content determination of materials," *Meas. Sci. Technol.*, vol. 21, pp. 1–26, 2010.

[15] U. Kaatze, "Techniques for measuring the microwave dielectric properties of materials," *Metrologia*, vol. 47, pp. S91–S113, 2010.

[16] J. Krupka, "Frequency domain complex permittivity measurements at microwave frequencies," *Meas. Sci. Technol.*, vol. 17, pp. R55–R70, 2006.

[17] J. Baker-Jarvis, M. D. Janezic, B. F. Riddle, R. T. Johnk, P. Kabos, C. L. Holloway, R. G. Geyer, and C. A. Grosvenor, "Measuring the permittivity and permeability of lossy materials: Solids, liquids, metals, building materials and negative index materials," NIST, Boulder, CO, NIST Tech. Note 1536, Feb. 2005.

[18] F. L. Penarada-Foix, P. J. Plaza-González, B. García-Baños, and D. Polo-Nieves, "A non-destructive method of measuring the dielectricand magnetic properties of laminate materials in open cavities," in *IEEE MTT-S Int. Microw. Symp. Dig.*, Fort Worth, TX, 2004, vol. 3, pp. 1821–1823.

[19] M. D. Janezic and J. Baker-Jarvis, "Full-wave analysis of a split-cylinder resonator for nondestructive permittivity measurements," *IEEE Trans. Microw. Theory Tech.*, vol. 47, no. 10, pp. 2014–2020, Oct. 1999.

[20] J. Baker-Jarvis, M. D. Janezic, P. D. Domich, and R. G. Geyer, "Analysis of an open-ended coaxial probe with lift-off for nondestructive testing," *IEEE Trans. Instrum. Meas.*, vol. 43, no. 5, pp. 711–718, Oct. 1994.

[21] A. Taflove, *Computational Electrodynamics: The Finite-Difference Time-Domain Method*. Norwood, MA: Artech House, 1995.

[22] J. Volakis, *Finite Element Method for Electromagnetics*. New York: IEEE Press, 1998.

[23] A. Wexler, "Solution of waveguide discontinuities by modal analysis," *IEEE Trans. Microw. Theory Tech.*, vol. MTT-15, no. 9, pp. 508–517, Sep. 1967.

[24] H. Patzelt and F. Arndt, "Double-plane steps in rectangular waveguides and their application for transformers, irises, and filters," *IEEE Trans. Microw. Theory Tech.*, vol. MTT-30, no. 5, pp. 771–776, May 1982.

[25] G. Conciauro, M. Guglielmi, and R. Sorrentino, *Advanced Modal Analysis*. New York: Wiley, 2000.

[26] J. A. Ruiz-Cruz, J. Esteban, and J. M. Rebollar, "Efficient boundary contour mode-matching method of H- and E-plane junctions by fast Fourier transform algorithm," *Proc. Inst. Elect. Eng.–Microw. Antennas Propag.*, vol. 150, no. 5, pp. 332–338, Oct. 2003.

[27] J. Gil, A. A. S. Blas, C. Vicente, B. Gimeno, M. Bressan, V. E. Boria, G. Conciauro, and M. Maestre, "Full-wave analysis and design of dielectric-loaded waveguide filters using a state-space integral-equation method," *IEEE Trans. Microw. Theory Tech.*, vol. 57, no. 1, pp. 109–120, Jan. 2009.

[28] J. Gil, A. M. Perez, B. Gimeno, M. Bressan, V. E. Boria, and G. Conciauro, "Analysis of cylindrical dielectric resonators in rectangular cavities using a state-space integral-equation method," *IEEE Microw. Wireless Compon. Lett.*, vol. 16, no. 12, pp. 636–638, Dec. 2006.

[29] J. Baker-Jarvis and B. F. Riddle, "Dielectric measurements using a reentrant cavity: Mode-matching analysis," NIST, Boulder, CO, NIST Tech. Note 1384, Nov. 1996.

[30] R. Lech and L. Mazur, "Analysis of circular cavity with cylindrical objects," *IEEE Trans. Microw. Theory Tech.*, vol. 55, no. 10, pp. 2115–2123, Oct. 2007.

[31] W. Xi and W. R. Tinga, "Field analysis of new coaxial dielectrometer," *IEEE Trans. Microw. Theory Tech.*, vol. 40, no. 10, pp. 1927–1934, Oct. 1992.

[32] J. Zheng and M. Yu, "Rigorous mode-matching method of circular to off-center rectangular side-coupled waveguide junctions for filter applications," *IEEE Trans. Microw. Theory Tech.*, vol. 55, no. 11, pp. 2365–2373, Nov. 2007.

[33] F. L. Penaranda-Foix, "Application of the generalized circuital analysis theory to the resolution of electromagnetic diffraction problems," (in Spanish) Ph.D. dissertation, Dept. Commun., Univ. Politécnica Valencia, Valencia, Spain, 2001.

[34] F. L. Penaranda-Foix and M. Ferrando-Bataller, "Scattering of inhomogeneous cylinders by circuital analysis," *Microw. Opt. Technol. Lett.*, vol. 39, no. 2, pp. 155–159, Oct. 2003.

[35] F. L. Penaranda-Foix, J. M. Catala-Civera, A. J. Canos-Marin, and P. J. Plaza-Gonzalez, "Solving cylindrically-shaped waveguides partially-filled with isotropic materials by modal techniques," in *Proc. 11th AMPERE*, Oradea, Romania, 2007, vol. 1, pp. 67–70.

[36] P. Arcioni, M. Bozzi, M. Bressan, G. Conciauro, and L. Perregrini, "Frequency/time-domain modelling of 3-D waveguide structures by a biRME approach. International journal of numerical modelling: Electronic networks, devices and fields," *Int. J. Numer. Modeling*, vol. 15, no. 1, pp. 3–21, 2002.

[37] P. Soto, V. E. Boria, J. M. Catalá-Civera, N. Chouaib, M. Guglielmi, and B. Gimeno, "Analysis, design, and experimental verification of microwave filters for safety issues in open-ended waveguide systems," *IEEE Trans. Microw. Theory Tech.*, vol. 48, no. 11, pp. 2133–2140, Nov. 2000.

[38] T. Sieverding and F. Arndt, "Field theoretical cad of open or aperture matched T-junction coupled rectangular waveguide structures," *IEEE Trans. Microw. Theory Tech.*, vol. 40, no. 2, pp. 353–362, Feb. 1992.

[39] J. M. Rebollar, J. Esteban, and J. E. Page, "Fullwave analysis of three and port–port rectangular waveguide junctions," *IEEE Trans. Microw. Theory Tech.*, vol. 42, no. 2, pp. 256–263, Feb. 1994.

[40] M. Ludovico, B. Piovano, G. Bertin, C. Zarba, L. Accatino, and M. Mongiardo, "CAD and optimization of compact ortho-mode transducers," *IEEE Trans. Microw. Theory Tech.*, vol. 47, no. 12, pp. 2479–2486, Dec. 1999.

[41] A. Alvarez, G. Connor, and M. Guglielmi, "New simple procedure for the computation of the multimode admittance or impedance matrix of planar waveguide junctions," *IEEE Trans. Microw. Theory Tech.*, vol. 44, no. 3, pp. 413–418, Mar. 1996.

[42] H. Kawabata, H. Tanpo, and Y. Kobayashi, "Analysis and experiments of a TM 010 mode cylindrical cavity to measure accurate complex permittivity of liquid," *IEICE Trans. Electron.*, vol. E87-C, no. 5, pp. 694–699, May 2004.

[43] H. Kawabata, Y. Kobayashi, and S. Kaneko, "Analysis of cylindrical cavities to measure accurate relative permittivity and permeability of rod samples," in *Proc. Asia–Pacific Microw. Conf.*, 2010, pp. 1459–1462.

[44] F. L. Penaranda-Foix and J. M. Catala-Civera, "Circuital analysis of cylindrical structures applied to the electromagnetic resolution of resonant cavities," in *Passive Microwave Components and Antennas*, 1st ed. Rijeka, Croatia: IN-TECH, Apr. 2010, ch. 7. [Online]. Available: http://sciyo.com/books/show/title/passive-microwave-components-and-antennas

[45] J. M. Rebollar and J. A. Encinar, "Field theory analysis of multiport-multidiscontinuity structures: An application to short-circuited E-plane septum," *Proc. Inst. Elect. Eng.—Microw. Antennas Propag.*, vol. 135, no. 1, pt. H, pp. 1–7, Feb. 1988.

[46] J. D. Wade and R. H. MacPhie, "Conservation of complex power technique for waveguide junctions with finite wall conductivity," *IEEE Trans. Microw. Theory Tech.*, vol. 35, no. 4, pp. 373–378, Apr. 1990.

[47] J. Krupka and J. Mazierska, "Contactless measurements of resistivity of semiconductor wafers employing single-post and split-post dielectric-resonator techniques," *IEEE Trans. Instrum. Meas.*, vol. 56, no. 5, pp. 1839–1844, Oct. 2007.

[48] C. A. Balanis, *Advanced Engineering Electromagnetics*. New York: Wiley, 1989.

[49] G. N. Watson, *A Treatise on the Theory of Bessel Funcions*. Cambridge, U.K.: Cambridge Math. Library, 1995.

[50] B. G. Korenev, *Bessel Functions and Their Applications*. New York: Taylor & Francis, 2002.

[51] G. G. Gentili, "Properties of TE–TM mode-matching techniques," *IEEE Trans. Microw. Theory Tech.*, vol. 39, no. 9, pp. 1669–1673, Sep. 1991.

[52] G. V. Eleftheriades, A. S. Omar, and L. P. B. Katehi, "Some important properties of waveguide junction generalized scattering matrices in the context of the mode matching technique," *IEEE Trans. Microw. Theory Tech.*, vol. 42, no. 10, pp. 1896–1903, Oct. 1994.

[53] R. E. Collin, *Foundations for Microwave Engineering*. Piscataway, NJ: IEEE Press, 2001.

[54] M. A. Leontovich, "On the approximate boundary conditions for electromagnetic fields on the surface of well conducting bodies," in *Investigations of Propagation of Radio Waves*, B. A. Vvdensky, Ed. Moscow, Russia: Acad. Sci. USSR, 1948, pp. 5–20.
[55] T. B. Senior, "Impedance boundary conditions for imperfectly conducting surfaces," *Appl. Sci. Res.*, vol. 8, pp. 418–436, 1960.
[56] R. F. Harrington, *Time–Harmonic Electromagnetic Fields*. New York: McGraw-Hill, 1961.
[57] F. L. Penaranda-Foix, J. M. Catala-Civera, A. J. Canos-Marin, and B. Garcia-Banos, "Circuital analysis of a coaxial re-entrant cavity for performing dielectric measurement," in *IEEE MTT-S Int. Microw. Symp. Dig.*, Boston, MA, 2009, vol. 1, pp. 1309–1312.
[58] W. Xi, W. R. Tinga, W. A. G. Voss, and B. Q. Tian, "New results for coaxial re-entrant cavity with partially filled gap," *IEEE Trans. Microw. Theory Tech.*, vol. 40, no. 4, pp. 747–753, Apr. 1992.
[59] M. Jaworski, "On the resonant frequency of a re-entrant cylindrical cavity," *IEEE Trans. Microw. Theory Tech.*, vol. MTT-26, no. 4, pp. 256–260, Apr. 1978.
[60] A. G. Williamson, "The resonant frequency and tuning characteristics of a narrow-gap re-entrant cavity," *IEEE Trans. Microw. Theory Tech.*, vol. MTT-24, no. 4, pp. 182–187, Apr. 1976.
[61] R. G. Carter, J. Feng, and U. Becker, "Calculation of the properties of reentrant cylindrical cavity resonators," *IEEE Trans. Microw. Theory Tech.*, vol. 55, no. 12, pp. 2531–2538, Dec. 2007.
[62] H. J. Eom, Y. C. Noh, and J. K. Park, "Scattering analysis of a coaxial line terminated by a gap," *IEEE Microw. Guided Wave Lett.*, vol. 8, no. 6, pp. 218–219, Jun. 1998.
[63] A. R. Weily and A. S. Mohan, "Rotationally symmetric FDTD for wideband performance prediction of TM01 DR filters," *Int. J. RF Microw. Comput.-Aided Eng.*, vol. 12, no. 3, pp. 259–271, 2002.
[64] C. Wang, K. A. Zaki, A. E. Atia, and T. G. Dolan, "Dielectric combline resonators and filters," *IEEE Trans. Microw. Theory Tech.*, vol. 46, no. 12, pp. 2501–2506, Dec. 1998.
[65] K. A. Zaki and C. Chen, "New results in dielectric-loaded resonators," *IEEE Trans. Microw. Theory Tech.*, vol. MTT-34, no. 7, pp. 815–824, Jul. 1986.
[66] J. C. Lagarias, J. A. Reeds, M. H. Wright, and P. E. Wright, "Convergence properties of the Nelder–Mead simplex method in low dimensions," *SIAM J. Optim.*, vol. 9, no. 1, pp. 112–147, 1998.
[67] A. J. Canos, J. M. Catala-Civera, F. L. Penaranda-Foix, and E. Reyes-Davo, "A novel technique for deembedding the unloaded resonance frequency from measurements of microwave cavities," *IEEE Trans. Microw. Theory Tech.*, vol. 54, no. 8, pp. 3407–3416, Aug. 2006.

Felipe L. Peñaranda-Foix (S'93–A'99–M'10) was born in Benicarló, Spain, in 1967. He received the M.S. degree in electrical engineering from the Universidad Politécnica de Madrid, Madrid, Spain, in 1992, and the Ph.D. degree in electrical engineering from the Universidad Politécnica de Valencia (UPV), Valencia, Spain, in 2001.

In 1992, he joined the Departamento de Comunicaciones, UPV, where he is currently a Senior Lecturer. He has coauthored approximately 40 papers in referred journals and conference proceedings and over 40 engineering reports for companies. He is a Reviewer for several international journals. His current research interests include electromagnetic scattering, microwave circuits and cavities, sensors, and microwave heating applications.

Dr. Peñaranda-Foix is an AMPERE member.

Michael D. Janezic (S'93–M'95–SM'02) received the B.S., M.S., and Ph.D degrees in electrical engineering from the University of Colorado at Boulder, in 1900, 1997, and 2003, respectively.

He is currently the Leader of the Advanced Materials Metrology Project (part of the Electromagnetics Division), National Institute of Standards and Technology (NIST), Boulder, Colorado. Since joining NIST in 1988, he has authored or coauthored over 50 papers that describe new techniques for measuring the high-frequency electromagnetic properties of materials, particularly low-loss dielectrics. His current research is focused on the development of accurate nondestructive measurement methods for determining the electromagnetic properties of dielectric and magnetic materials at microwave and millimeter-wave frequencies.

Dr. Janezic was the recipient of the NIST Bronze Medal in 2005 for the development of nondestructive test methods for measuring the complex permittivity of low-loss dielectric substrates at microwave frequencies.

Jose M. Catala-Civera (M'04) was born in Valencia, Spain, in February 1969. He received the Dipl. Ing. and Ph.D. degrees from the Universidad Politécnica de Valencia, Spain, in 1993 and 2000, respectively.

Since 1996, he has been with the Communications Department, Universidad Politécnica de Valencia, where he received the Readership in 2000, becoming a Full Professor in 2011. He is currently Co-head of the Microwave Applications Research Division, Instituto de Aplicaciones de las Tecnologias de la Informacion y de las Comunicaciones Avanzadas (ITACA), Universidad Politécnica de Valencia. He has coauthored over 100 papers in referred journals and conference proceedings and over 50 engineering reports for companies. He is a reviewer of several international journals. He holds 18 patents. His research interests encompass the design and application of microwave theory and applications, the use of microwaves for electromagnetic heating, microwave cavities and resonators, measurement of dielectric and magnetic properties of materials, and development of microwave sensors for nondestructive testing.

Dr. Catala-Civera is currently a board member of the Association of Microwave Power in Europe for Research and Education (AMPERE), a European-based organization devoted to the promotion of RF and microwave energy.

Antoni J. Canos was born in Almenara (Castelló de la Plana), Spain, in 1973. He received the Dipl. Eng. and M.S. degrees in electrical engineering from the Universitat Politècnica de València, Valencia, Spain, in 1999 and 2003, respectively, and is currently working toward the Ph.D. degree at the Universitat Politècnica de València.

In 2001, he joined the Instituto de Aplicaciones de las Tecnologias de la Informacion y de las Comunicaciones Avanzadas (ITACA), Valencia, Spain, as a Research and Development Engineer. Since 2005, he has been an Assistant Professor with the Communications Departament, Universitat Politècnica de València. His current research interests include numerical analysis and design of waveguide components, microwave measurement techniques and devices for the electromagnetic characterization of materials, noninvasive monitoring of processes involving dielectric changes, and design of low-cost vector network analyzers.